Available online at www.sciencedirect.com
ScienceDirect
Chinese Journal of Aeronautics 22(2009) 301-306
Chinese Journal of Aeronautics
www.elsevier.com/locate/cja

Method of Passive Image Based Crater Autonomous Detection

Ding Meng[a,*], Cao Yunfeng[a,b], Wu Qingxian[a]

[a]*College of Automation Engineering, Nanjing University of Aeronautics and Astronautics, Nanjing 210016, China*

[b]*Academy of Frontier Science, Nanjing University of Aeronautics and Astronautics, Nanjing 210016, China*

Received 23 May 2008; accepted 12 January 2009

Abstract

Impact craters are commonly found on the surface of planets, satellites, asteroids, and other solar system bodies. The application field of crater detection algorithm ranges from estimation of planetary surface age to autonomous landing on planets and advanced statistical analyses. this article introduced a method of passive image based crater autonomous detection. Candidate area, is defined as a small rectangular region including craters. The criterion to select a candidate area is there being one or a few craters in it. Then after a brief discussion of pre-processing of crater candidate area to obtain edge information of craters, comes a description of the theory of chord midpoint Hough transform and the process of crater detection. The article analyzes the reason behind the production of false center points of circularity as well. Experiment evidences the viability of discovering relatively large craters with clear edges.

Keywords: passive image; crater detection; autonomous detection; chord midpoint; Hough transform

1. Introduction

Impact craters widely spread and can be frequently found on the surfaces of planets, satellites, asteroids, and other solar system celestial bodies. Their number, distribution, pattern, morphology and size can be determined by means of passive images. With the help of the data from the images, the age of the surface or surface units and the relative age of different bodies can be identified[1-3]. Craters also serve as convenient reference objects for visual motion estimation. Optical landmark navigation by guidance of craters on the surface of a central body was first put into operation by the near Earth asteroid rendezvous (NEAR) to meet with asteroid Eros 433 in February 2000. Successful fulfillment of NEAR mission has proven that crater tracking is a powerful tool for spacecraft orbit determination in low altitude orbits[4]. On the other side, it is also important to develop a crater detection algorithm to avoid probe hazards[5-6].

Images can be obtained by different sensors, which include active sensors and passive sensors. Light detection and ranging (LIDAR) and phased array terrain radar (PATR) belong to the former while digital cameras latter. Active sensors are preferable because they are capable of taking direct measurement of the depth of sensed terrain, and show less sensitivity to atmospheric opacity. Also, the algorithm to interpolate these data is characterized by relative simplicity and rapidity in operation. However, apart from greater expense, larger weight (6-25 kg) and higher power consumption (40-200 W), active sensors are deficient in low resolution (40×40-100×100), narrow field of view (FOV) (15°-40°) and high volume (2-40 L). On the contrary, cameras have advantages in light weight (0.3 kg), less power consumption(13 W), higher resolution (1 024×1 024), wide FOV(120°), low volume (2 L) and a greater sensing range[7].

Because of greater importance of passive image based crater detection, many researchers from different countries have paid much more attention to it and several algorithms have been published. Generally, the algorithms of autonomous crater detection can be classified into three categories: unsupervised (fully autonomous)[8-10], supervised (machine learn)[11-13] and compound (combining unsupervised and supervised)[14-16].

The method proposed in this article is built on the chord midpoint Hough transform (CMHT) and a classic unsupervised or fully autonomous crater detection algorithm. The unsupervised methods apply pattern recognition techniques to detect craters according to the geometric features of craters, such as circularity or ellipse. Currently, detection can be conducted with the

*Corresponding author. Tel.: +86-25-84896392.
E-mail address: nuaa_dm@hotmail.com
Foundation items: Innovation Fund for Graduate Student of Jiangsu (CX07B_113z); Innovation Fund for Ph.D. of Nanjing University of Aeronautics and Astronautics (BCXJ07-06)

1000-9361/$ - see front matter
doi: 10.1016/S1000-9361(08)60103-X

approaches of Hough transform (HT) and other improved methods[12,17]. Because of the complexity of parameter space, traditional Hough transform is difficult to finish ellipse or circularity extraction. Therefore, some geometric constraints are imposed to reduce the complexity of parameter space, such as geometric property-based method[18] or K-RANSAC-based method[19]. CMHT-based method[20] in this article is built on the fact that a chord passing through the center of an ellipse or circularity is divided into bisection. According to this geometric constraint, the center point of ellipse or circularity is detected firstly followed by computing other parameters.

The supervised methods use machine learning conception to construct classifiers and train an algorithm to detect craters. The compound methods combine more than one algorithm inclusive of unsupervised and supervised to improve results of crater detection.

Generally, the main process of crater detection includes candidate area (CA) selection, pre-processing and crater detection. Section 2 is limited to demonstrate candidate area selection and Section 3 to pre-processing of candidate area. Section 4 introduces chord midpoint Hough transform-based crater detection in detail. Section 5 presents experimental results and analysis thereof and Section 6 gives out the conclusions.

2. Candidate Area Selection

By candidate area is meant a small rectangular region including craters. The criterion to select a candidate area is there being one or more craters in it. This article incorporates Bandeira's edge detection-based method[21-22] with Kanade-Lucas-Tomasi (KLT) feature point detection-based method[23] in candidate area selection. With the algorithm having already been well documented, Fig.1 shows the results of the candidate area selection with eight areas chosen, one area containing two craters, two areas no crater at all and five areas only one crater each.

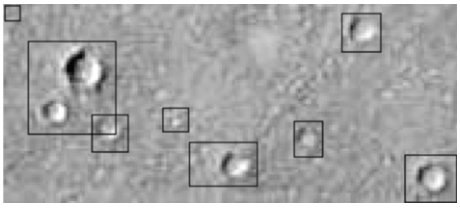

Fig.1 Candidate area selection.

3. Pre-processing of Candidate Area

The first step of geometric shape extraction algorithm based on Hough transform and the improved method is to process original image and obtain edge information. The purpose of pre-processing of candidate areas is also for clarifying the crater edge.

A typical crater in the image is characterized by an elliptical or circular shape and a shadowed area changing from bright to dark, and inside it the image intensity should present to be monotonously decreasing along the light direction. Therefore, on gray-level images of planetary surfaces, intensity variations are strong in the region of craters. In fact, most common edge detection operators based on gradient variance (e.g. Canny and Sobel) do not achieve good results for crater edge detection[21].

Ref.[22] introduced an algorithm and the goal was the detection and enhancement of significant local variations in the gray level, which denounced the presence of shadows due to crater rims. This algorithm simply includes following steps:

Step 1 A mask M with $n \times n$ elements is centered at each pixel of the original image. Create a new image A and every pixel A_{uv} calculated by $A_{uv}=\max[m(M)-\min(M), \max(M)-m(M)]$, $m(\cdot)$ means the local mean.

Step 2 Find threshold $T=\alpha[\max(A)-\min(A)]+\min(A)$, where α, as a coefficient chosen for different images, is very important, for it is closely linked to image noise and high-frequency signal. High value of α will lead to effective elimination of noise on the credit side, but deletion of edges of small craters on the flip side.

Step 3 The threshold T is applied to each pixel A_{uv} of A to compute the value (0 or 1) that will be assigned to each new pixel B_{uv} in the resultant binary image B.

Step 4 Closing operator of morphological image proces sing fuses narrow breaks and long, thin gulfs, eliminates small holes and fills gaps in the contour.

This article chooses from Fig.1 one candidate area with two craters to implement the edge extraction. Fig.2 shows the result ($\alpha = 0.4$).

Fig.2 Edge extraction ($\alpha = 0.4$).

From Fig.2, it is found that the edge of crater is relatively wide, which will make Hough transform more difficult in the next step. For this reason, this article tries to use mid axis transform, a thinning algorithm of morphological image processing, to extract skeletons of edge. This step is helpful for speeding up computation and improving reliability of crater detection (see Fig.3).

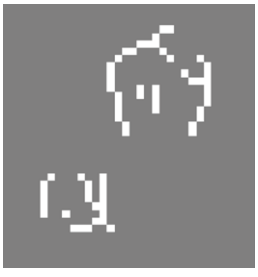

Fig.3 Edge skeletons of crater.

4. Crater Detection

4.1. CMHT

Hough first put forward HT for line searching in 1962. The computational attractiveness of the HT arises from subdividing the parameter space into so-called accumulator cells. The complexity of traditional HT entails a strenuous computational work. Therefore, it is difficult for traditional HT to carry out successful circularity detection because the parameter space of circularity is of high dimension (3D). At present, many algorithms have introduced methods to reduce dimensions of parameter space and many researchers have paid attention to finding the location of center point based on geometric constraints.

Ref.[20] has demonstrated a method of ellipse or circularity extraction based on CMHT, which is established on dividing the chord passing through the center of an ellipse or circularity into bisection. This algorithm introduced the concept of "inscribed ellipse", by which is meant a new ellipse constituted by the midpoint of chord which is constructed one point of ellipse or circularity connect with other points belonging to this ellipse or circularity. A theorem is provided below, but its proof is omitted here.

Theorem One point through which every chord of ellipse or circularity passes is divided into bisection on the plane is the center point of this ellipse or circularity.

This is the theorem that CMHT is built on. In the binary images inclusive of ellipse or circularity, all inscribed ellipses must pass through the center of ellipse or circularity, and the chord midpoint which is so constructed that it does not belong to ellipse or circularity is difficult to pass through the center of ellipse or circularity. It is convenient to set accumulator space for CMHT and obtain the location of center point of ellipse or circularity based on this theorem.

4.2. CMHT-based crater detection

The key of CMHT-based crater detection is to find the center point of a crater, of which the process can be described as follows:

Step 1 Scan whole binary image matrix, store location parameters of the edge point and build 2D accumulator space which represents the location of midpoint.

Step 2 Compute accumulator according to CMHT. For every detected point, scan all other edge points, compute the midpoint and add 1 to the corresponding accumulator cell (location of midpoint). For reducing computation work, the point that has been scanned will not enter the new round of location computation.

Step 3 Find the center point. Set a threshold, if the number of accumulator cell is larger than the threshold, this cell becomes the candidate center point. Search each connected domain for the center point and confirm the center location by the maximum value of accumulator of each connected domain.

Now, the validity of this method of center point detection has been confirmed. There are two main factors to influence validity of CMHT-based center point detection: random noise and pixel points belong to different ellipse or circularity. First, random noise is known and can be reduced by some filters. The second factor is implicit and it could not be removed or reduced. Fig.4 shows two identical circularities without noise, where "。" means candidate center point by CMHT. The number of center points belonging to the left circularity is 5 and that the right 5. The number of false center points is 24, which could be simply blamed for the fact that they are corporate center points of ellipse constructed by two rims which has relatively long distance and conic constructed by two rims which has relatively short distance. Table 1 lists maximum values of accumulators of three single connected domains.

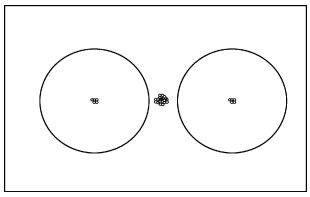

Fig.4 Distribution of center points (threshold=35).

Table 1 Location of center points

Location of center point	Number of accumulator
(51, 55)	134
(91, 55)	265
(130, 55)	133

For convenience of description, in this article the edges under discussion are limited to circular craters. After finishing center point search, radius of circularity must be computed. For every detected center point(x_0^i, y_0^i), a new coordinate system(x'^i, y'^i) should be built through the following transformation:

$$\begin{cases} x^i = x'^i + y_0^i \\ y^i = y'^i + y_0^i \end{cases}$$

where (x^i, y^i) is original coordinate system.

In the new coordinate system, find out the points symmetrical to the origin, set up 1D accumulator space to determine radius, scan this accumulator to fix the radius based on the maximum value of accumulator.

After computing all parameters, the false circularities should be deleted. By false circularity is meant the detected circularity, of which, the ratio between edge points and the points belonging to it is less than a given threshold.

5. Experiments and Analysis

Fig.1 provides a reference for comparison in the experiment. Through candidate area selection, only

one candidate area is left with two craters in it. Fig.5 shows its CMHT-based accumulator.

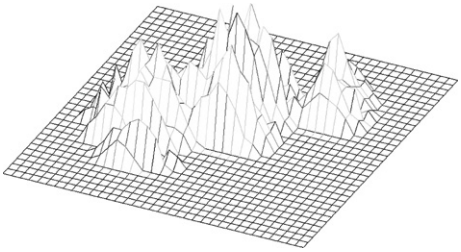

Fig.5 Status of accumulator.

According to this accumulator and the given threshold, the connected domains are confirmed as shown in Fig.6. There are five connected domains of center points. Table 2 lists the parameters of those connected domains. In each connected domain, the maximum coordinate of accumulator is selected as the center point.

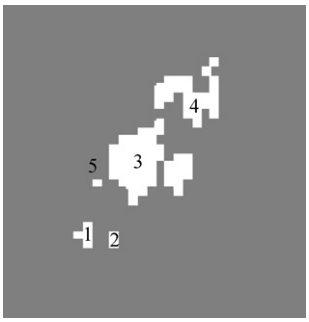

Fig.6 Connected domains of center points.

Table 2 Parameters of connected domains

Connected area	Acreage/ pixel	Location of center point	Number of accumulator
1	4	(10,27)	15
2	2	(13,27)	12
3	37	(17,17),(16,18),(17,19)	23
4	23	(21,10),(21,12)	18
5	1	(11,21)	10

After center point detection, compute radius of every crater. Figs.7-8 illustrate the final results of the candidate area with two craters in it and those of the area shown in Fig.1 respectively. Fig.9(a) and Fig.9(b) show crater detection results of two images with low and high resolution.

In order to make a quantitative assessment of the autonomous crater detection, two detection rate parameters, the true detection rate TDR_p and the false detection rate FDR_p, are used and computed as follows:

$$TDR_p = \frac{TD_p}{TN} \times 100\%$$

$$FDR_p = \frac{FD_p}{TD_p + FD_p} \times 100\%$$

where TD_p is the number of true detections, FD_p the number of false detections and TN the total number of craters in one region. Table 3 presents TDR_p in Fig.9.

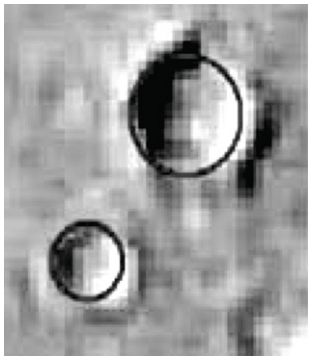

Fig.7 Final results of candidate area with two craters in it (radius is 6,12, threshold of false circularity is 0.6).

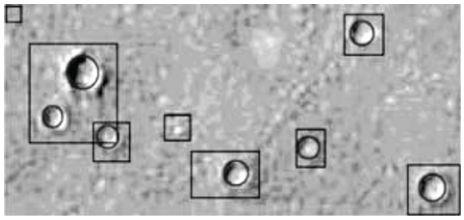

Fig.8 Final results of the area shown in Fig.1 with 7 craters detected.

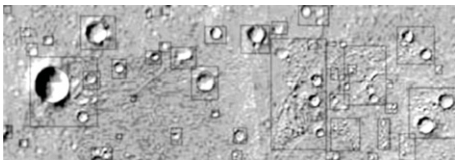

(a) A low resolution image(threshold of false circularity is 0.7)

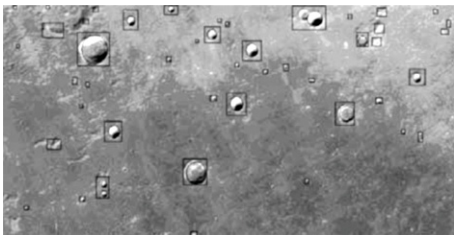

(b) A high resolution image(threshold of false circularity is 0.6)

Fig.9 Crater detection results.

Table 3 TDR_p of Fig.9

Region	CA number	TD_p	TN	TDR_p/%
Fig.9(a)	46	19	24	79
Fig.9(b)	46	14	18	78

By analyzing Table 3, three conclusions for this crater detection algorithm could be drawn as follows:

(1) Craters are completely involved in the image, which means that incomplete craters can not be detected with this algorithm.

(2) Craters must have clear edges that could be brought out in the image (in Table 3, TN is the number of craters having clear edges), which means that old craters with blurred edges must be shunned out of the

usage of the approach. This is the prerequisite for all detection algorithms based on edge information.

(3) Some small craters might not be detected under certain circumstances. For example, for two craters with quite large difference in size in one candidate area, the smaller one might not be discovered.

Furthermore, TDR_p is strongly correlated to the candidate area selection. If some crater fails to be included in any one of candidate area, it could not be detected at all. In authors' experiences, the correct rate of candidate area selection is more than 95% in a simple terrain which accords with Fig.9.

Generally, FDR_p is only related to some candidate areas where there are more than one craters. In fact, false detected craters are the false circularities which have been introduced in Section 4.2. Fig.10 shows the variation of FDR_p of images shown in Fig.9(a) and Fig.9(b) against threshold of false circularity. From Fig.10, it could be found that FDR_p pertinent to Fig.9(a) goes higher than Fig.9(b) because, compared to Fig.9(a), Fig.9(b) has less candidate areas which include craters and, moreover, higher resolution.

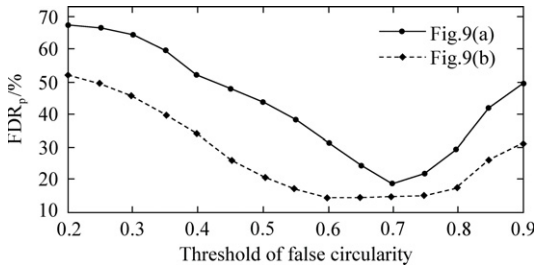

Fig.10 Variation of FDR_p of images in Fig.9 against threshold of false circularity.

6. Conclusions

Generally, passive imaging based autonomous craters detection is difficult to be applied in practices because of the changeability in appearance of craters and surrounding terrain. A lot of experiments show that the unsupervised methods work well with relatively large craters having clear edge information, but their efficiency declines as the complexity of the terrain increases.

Compared with other similar algorithms, the proposed algorithm has two main characteristics: First, by introducing candidate area selection to divide whole image into many different small regions, the complexity of the terrain around detected craters could be decreased. Besides, by using CMHT-based algorithm to compute small regions, the computation speed and reliability of crater detection could be improved. Second, as the center point detection is the key of the proposed method, the real center point of a crater can be detected effectively by obtaining maximum of accumulator of single connected domain, which, thereby, makes the strenuous computation work much easier.

References

[1] Tanaka K L. The stratigraphy of Mars. J Geophys Res 1986; 91(B13): E139-E158.

[2] Neukum G, Konig B, Arkani-Hamed J. A study of lunar impact crater size-distributions. Earth, Moon, and Planets 1974; 12(2): 201-229.

[3] Tompkins S, Pieters C M. Mineralogy of the lunar crust: results from clementine. Meteorit Planet Sci 1999; 34(1): 25-41.

[4] Cheng Y, Johnson A E, Matthies L H, et al. Optical landmark detection for spacecraft navigation. Proc of the 13th AAS/AIAA Space Flight Mechanics Meeting. 2003; 114: 1785-1803.

[5] Cheng Y, Miller J K. Autonomous landmark based spacecraft navigation system. Proc of the 13th AAS/AIAA Space Flight Mechanics Meeting. 2003; 114: 1769-1783.

[6] Johnson A E, Cheng Y, Matthies L H. Machine vision for autonomous small body navigation. 2000 IEEE Aerospace Conference. 2000; 7: 616-671.

[7] Huertas A, Cheng Y, Madison R. Passive imaging based multi-cue hazard detection for spacecraft safe landing. 2006 IEEE Aerospace Conference. 2006.

[8] Bue B D, Stepinski T F. Machine detection of Martian impact craters from digital topography data. IEEE Trans Geosci Remote Sens 2007;45(1):265-274.

[9] Flores-Méndez A. Crater marking and classification using computer vision. In: Sanfeliu A, Ruiz-Shulcloper J, ed. Progress in Pattern Recognition, Speech and Image Analysis: Lecture Notes in Computer Science. New York: Springer-Verlag, 2003; 79-86.

[10] Michael G. Coordinate registration by automated crater recognition. Planetary Space Sci 2003; 51(9): 563-568.

[11] Burl M C, Stough T, Colwell W, et al. Automated detection of craters and other geological features. 〈http://hdl. handle. net/2014/12751〉. Proc Int Symp Artif Intell, Robot and Autom in Space. 2001.

[12] Vinogradova T, Burl M, Mjosness E. Training of a crater detection algorithm for Mars crater imagery. Proc IEEE Aerosp Conf. 2002; 7: 3201-3211.

[13] Wetzler P G, Enke B, Merline W J, et al. Learning to detect small impact craters. Proc 7th IEEEWACV/ MOTION. 2005; 1: 178-184.

[14] Magee M, Chapman C R, Dellenback S W, et al. Automated identification of Martian craters using image processing. 〈http://www.1pi.usra.edu/meetings/ 1psc2003/pdf/1756.pdf〉. Lunar and Planetary Science XXXIV, 2003.

[15] Earl J, Chicarro A F, Koeberl C, et al. Automatic recognition of crater-like structures in terrestrial and planetary images. 〈http://earth.esa.int/rtd/Articles//Lunar_Planetary Science.pdf〉. Lunar and Planetary Science XXXVI, 2005.

[16] Bandeira L, Saraiva J, Pina P. Development of a methodology for automated crater detection on planetary images. Proc Iberian Conf Pattern Recog Image Anal. 2007; 4477: 193-200.

[17] Homma K, Yamamoto H, Isobe T, et al. Massively parallel processing for crater recognition. 〈http://www.lpi. usra.edu/meetings/lpsc97/pdf/1073.pdf 〉. Lunar and Planetary Science XXVIII, 1997.

[18] Yang Z G, Luan X M, Hu H. Ellipse extraction using

geometric properties. Journal of Harbin Engineering University 1997; 18(5): 70-77. [in Chinese]
[19] Yang Z G, Ma Y. A new method for ellipse detection using K-RANSAC based on generalized orthogonality principle. Acta Automatica Sinica 2002; 28(4): 520-526. [in Chinese]
[20] Qu W T. Chord midpoint Hough transform based elipse detection method. Journal of Zhejiang University (Engineering Science) 2005; 39(8): 1132-1135. [in Chinese]
[21] Bandeira L, Saraiva J, Pina P. Enhancing impact crater rims to increase recognition rates. Proc VISAPP. 2006; 407-412.
[22] Bandeira L, Saraiva J, Pina P. Impact crater recognition on Mars based on a probability volume created by template matching. IEEE Trans Geosci Remote Sens 2007; 45(12): 4008-4014.
[23] Tissainayagam P. Assessing the performance of corner detectors for point feature tracking applications. Image and Vision computing 2004; 22(8): 663-679.

Biographies

Ding Meng Born in 1981, he received B.S. and M.S degrees from the College of Automation Engineering, Nanjing University of Aeronautics and Astronautics in 2003 and 2006 respectively. He is currently working toward Ph.D. degree in the same university. His academic interests lie in application of computer vision and pattern recognition to aerospace exploration.
E-mail: nuaa_dm@hotmail.com

Cao Yunfeng Born in 1964, he received M.S. degree in College of Automation Engineering, Nanjing University of Aeronautics and Astronautics in 1992. Now, he is the professor in Academy of Frontier Science of Nanjing University of Aeronautics and Astronautics. His academic interests lie in flight control system and intelligence control.
E-mail: cyfac@nuaa.edu.cn

Wu Qingxian Born in 1955, he received M.S. degree from Southeast University in 1985. Now, he is a professor in College of Automation Engineering of Nanjing University of Aeronautics and Astronautics. His academic interests lie in intelligence control and pattern recognition.
E-mail: wuqingxian@nuaa.edu.cn